Applied Surface Science 419 (2017) 429–438

Contents lists available at ScienceDirect

Applied Surface Science

journal homepage: www.elsevier.com/locate/apsusc

Full Length Article

Fabrication of PVDF-based blend membrane with a thin hydrophilic deposition layer and a network structure supporting layer via the thermally induced phase separation followed by non-solvent induced phase separation process

Zhiguo Wu[a], Zhenyu Cui[a,*], Tianyu Li[a], Shuhao Qin[b], Benqiao He[a], Na Han[a], Jianxin Li[a]

[a] State Key Laboratory of Separation Membranes and Membrane Processes, School of Material Science and Engineering, Tianjin Polytechnic University, Tianjin 300387, PR China
[b] National Engineering Research Center for Compounding and Modification of Polymer Materials, Guiyang 550014, PR China

ARTICLE INFO

Article history:
Received 20 December 2016
Received in revised form 17 February 2017
Accepted 7 May 2017
Available online 8 May 2017

Keywords:
Thermally induced phase separation
Non-solvent induced phase separation
Blend
Surface deposition
Crystallization control

ABSTRACT

A simple strategy of thermally induced phase separation followed by non-solvent induced phase separation (TIPS-NIPS) is reported to fabricate poly (vinylidene fluoride) (PVDF)-based blend membrane. The dissolved poly (styrene-co-maleic anhydride) (SMA) in diluent prevents the crystallization of PVDF during the cooling process and deposites on the established PVDF matrix in the later extraction. Compared with traditional coating technique, this one-step TIPS-NIPS method can not only fabricate a supporting layer with an interconnected network structure even via solid-liquid phase separation of TIPS, but also form a uniform SMA skin layer approximately as thin as 200 nm via surface deposition of NIPS. Besides the better hydrophilicity, what's interesting is that the BSA rejection ratio increases from 48% to 94% with the increase of SMA, which indicates that the separation performance has improved. This strategy can be conveniently extended to the creation of firmly thin layer, surface functionalization and structure controllability of the membrane.

1. Introduction

The membrane separation technique has been extensively used for water treatment during the past few decades [1]. The thin skin layer, well-interconnected supporting layer and good hydrophilicity positively contribute to high permeability and good antifouling of the membrane [2]. It is well known that the membrane structures of the skin layer and the supporting layer are influenced by the method of preparation. Non-solvent induced phase separation (NIPS) [3] and thermally induced phase separation (TIPS) [4], based on mass transfer and heat transfer, respectively, are the two methods used to prepare commercial membranes. Compared with membranes prepared using NIPS, the membrane prepared via TIPS has certain advantages, such as better mechanical strength, narrower pore size distribution and less controlling parameters [5]. However, the network structure suitable for filtration is usually obtained through spinodal decomposition (SD), which occurs at high temperature, i.e., usually higher than the melting temperature of polymer [6]. The high temperature leads to the decomposion of the polymer and hydrophilic additive, volatilization of diluent and high energy consumption. Thus, it is imperative to explore new method to obtain this kind of network structure in lower temperature.

Poly (vinylidene fluoride) (PVDF) is an excellent membrane material due to its high mechanical strength, good thermal stability and chemical resistance [5]. However, natural hydrophobicity makes it prone to foul in a water treatment. Many approaches, such as plasma treatment [7], surface coating [8–10] and blending with amphiphilic copolymers [11] or inorganic nanoparticles [12], have been considered to improve the hydrophilicity of the PVDF membrane. However, for the PVDF fabricated by TIPS, most researches have been focusing on adjusting the membrane structure by selecting novel diluent [13,14] or mixed diluent [15] and few studies concentrated on the hydrophilic modification of PVDF. Rajabzadeh [16] and Qin [17] used Polyvinyl Pyrrolidone (PVP) and silicon dioxide (SiO_2) to improve the hydrophilicity of PVDF membrane, respectively. Nevertheless, the decomposition of PVP at higher temperature and the agglomeration of inorganic nanoparti-

* Corresponding author.
E-mail address: cuizheyhh@163.com (Z. Cui).

http://dx.doi.org/10.1016/j.apsusc.2017.05.059
0169-4332/

cle are unavoidable in the membrane fabrication process. And also they can be easily fall off when used in water treatment.

Poly (styrene-co-maleic anhydride) (SMA) is a type of amphiphilic copolymer which has been widely used as a functional or hydrophilic additive via NIPS [18–20]. The hydrophilic group of the amphiphilic copolymer segregates towards the membrane surface, known as surface segregation, during the progress of membrane formation, thus enhancing the antifouling of the membrane. However, the effect of surface segregation of the amphiphilic copolymer by NIPS is reduced for the no-polar low surface energy segment due to the unfavourable thermodynamics [11].

Our previous study showed that the morphology of the membrane changes from cellular structure to network structure and corresponding membrane formation mechanism changes from liquid–liquid (L-L) to solid-liquid (S-L) via TIPS with the addition of PMMA [21]. This indicates that the interaction between polymers [22] has a remarkable effect on the membrane formation progress in the TIPS process. And SMA is partially compatible with PVDF because the segments of styrene and C=O in SMA have a suitable interaction with fluorine in PVDF [23]. Thus, blending SMA will enhance hydrophilicity of the membrane and exert effect on the membrane formation process in a different way compared with PMMA. Herein, we report a simple technique to fabricate PVDF/SMA blend membrane via the thermally induced phase separation followed by non-solvent induced phase separation (TIPS-NIPS) process. In detail, a suitable high boiling point organic reagent, acetyl tributyl citrate (ATBC), which can be used as both the solvent of SMA and the diluent of PVDF, was selected. PVDF would crystallize, but SMA would still solve in ATBC during the cooling process, and SMA would deposit on the surface and pore of the established PVDF matrix during the extraction process. Unlike surface segregation and surface coating, this membrane formation mode of surface deposition is equal to coat a skin of SMA on both the surface and the inner part of the established PVDF matrix. In addition to the surface functionalization or hydrophilicity of the membrane, the membrane structure is also controlled by the interaction between the PVDF and the SMA. The membrane formation mechanism and the effect of the SMA on the membrane structure and separation performance are discussed in detail.

2. Experimental section

2.1. Materials

The PVDF ($M_w = 6.85 \times 10^5$) and SMA (random copolymer, $M_w = 1.2 \times 10^5$, MA = 26 wt.%) were purchased from Solvay Silexis (Belgium) and Polyscope (Geleen, Netherlands), respectively. They were dried in a vacuum oven at 50 °C for 48 h prior to use. The ATBC was purchased from Jiangsu Lemon Chemical & Technology Co., Ltd (Jiangsu, P.R. of China) and was used as a diluent without further purification. The bovine serum albumin (BSA) was purchased from the Institute of Haematology, Chinese Academic of Medical Sciences (Tianjin, P.R. of China). Ethanol (purity > 99%) was used as the extractant.

2.2. The phase diagram of PVDF/SMA/ATBC system

The sample was prepared using the previous method [22]. The measured PVDF, SMA and ATBC, as presented in Table 1, were put into the vessel, stirred and heated to 180 °C in a closed condition to form a homogenous solution (system code denoted by m). To solidify the solution, it was quenched in liquid nitrogen. The solidified sample was chopped into small pieces and placed between a pair of microscope cover slips, and the sample was then heated on a LK-600 pH hot stage (LINKAM THMS 600) to 180 °C and maintained at that temperature for 3 min to erase thermal history. It was then cooled to 25 °C at 10 °C min^{-1}. The cloud point temperature (T_{cloud}) was determined visually by the appearance of turbidity under a polarizing optical microscope (POM, BX51C, Olympaus, Japan).

Differential scanning calorimeter (DSC, 204F1, Germany) was used to determine the crystallization temperature (T_c) of the PVDF/SMA/ATBC system. Approximately 10 mg of the solidified sample was sealed in an aluminium pan, melted at 180 °C for 3 min and then cooled to 25 °C at 10 °C min^{-1}. The onset temperature of the exothermic peak was taken as T_c.

2.3. Preparation of PVDF/SMA blend membrane

The blend membrane was prepared using the previous method [22]. The PVDF/SMA/ATBC solidified sample prepared as described in 2.2 was chopped into small pieces and compressed in a mould at 180 °C to form a thin film. After the mould was quenched in water bath (25 °C), the ATBC was extracted with ethanol for 24 h. The final blend membrane (the membrane code denoted by M) was vacuum freeze-dried for 12 h.

Dynamic mechanical thermal analysis (DMA, 242C, Germany) was used to investigate the compatibility between PVDF and SMA. The PVDF/SMA membrane was cut into rectangular samples (20 mm long and 3 mm wide) and measured in the dynamic tension deformation mode, whereas the SMA powder was measured in the dynamic compression deformation mode. The DMA measurement was performed in isochronal conditions (frequency 1 Hz) at a temperature range between −50 °C and 200 °C and heating rate of 5 °C min^{-1}.

2.4. Characterization of PVDF/SMA membrane

The surface composition of membranes was analysed using X-ray photoelectron spectroscopy (XPS, K-Aepna, USA) and attenuated total reflectance Fourier Transform Infrared Spectroscopy (ATR-FTIR, TENSOR37, Germany). For the XPS measurement, survey spectra over a range of 0 to1100 eV and high-resolution spectra of C_{1s} peak were collected. For ATR-FTIR, spectrophotometry with ZnSe as an internal reflection element was used. The cross-section of the membrane for the transmission electron microscopy (TEM, H-7650, HITACHI, Japan) test was prepared as follows. First, the membrane of the desired size was embedded in the Glaubert Araldite embedding epoxy resin with a cross-linker, accelerator and plasticizer using standard embedding protocol. The embedding medium was hardened at 60 °C for 48 h and sectioned to approximately 90 nm thick slices using an ultramicrotome (Reichert-Jung Ultracut E). The membrane was then transferred to the TEM grids and dyed using phosphotungstic acid (C=O in SMA can be dyed using phosphotungstic acid but PVDF cannot). Finally, the slices were examined on the TEM.

The cross-section and surface morphologies of the membrane were sputtered with gold and observed by scanning electron microscopy (SEM, OLYMPUS, Japan). The cross-section of the membrane was obtained by freeze-fracturing in liquid nitrogen.

The surface roughness of the membrane was examined using an atomic force microscope (AFM, CSPM5500) operated in a tapping mode using silicon tips (BS-Tap300, Al coating, Nanoscience Instruments) with radius of 10 nm.

The pore size and its distribution was calculated by surface SEM image [24] and porosity of the membrane was measured by comparing the weight membrane before and after immersion into

Table 1
The casting solution, DMA and DSC date of PVDF/SMA blending membrane.

Membrane code	Casting solution			DMA			DSC[a]			
	PVDF[wt.%]	SMA[wt.%]	ATBC[wt.%]	T_α(PVDF)	T_{SMA}	ΔT	T_m^{oneset} [°C]	T_m^p [°C]	T_m^f [°C]	ΔT_m [°C]
M0	20	0	80	55.0			153.1	170.6	179.2	20.3
M1	20	1	79	111.7	172.0	60.3	156.3	169.4	173.6	17.3
M2	20	2	78	114.2	177.0	62.8	161.2	169.1	174.8	12.6
M3	20	3	77	104.4	177.8	73.4	164.4	168.9	174.9	11.2
M4	20	4	76	111.0	176.8	65.8	162.6	169.4	175.9	11.6
M5	20	5	75	105.7	168.5	62.8	164.5	170.6	175.7	12.2
M6	20	6	74	113.6	167.8	54.2	158.7	172.3	175.9	17.9
M7	20	7	73	118.0	172.0	54.0	158.9	172.6	178.7	18.1

a) T_m^{oneset}, melting onset temperature, T_m^p, melting peak temperature, T_m^f, melting ending temperature, ΔT_m, width of melting peak

n-butanol [22]. The porosity was calculated using the following equation:

$$p\% = \frac{\frac{M_b}{\rho_b}}{\left(\frac{M_p}{\rho_p}\right) + \left(\frac{m_b}{\rho_b}\right)} \times 100$$

where P% is the porosity of membrane, M_p is the mass of membrane, M_b is the mass of absorbed *n*-butanol, ρ_p and ρ_b are the density of the membrane and the *n*-butanol, respectively.

The crystallization behavior of the membrane was studied with a differential scanning calorimeter (DSC204F1, Germany). Approximately 10 mg of the membrane was sealed in an aluminium pan and then heated from 20 °C to 200 °C at a rate of 10 °C min^{-1}.

2.5. The hydrophilicity of PVDF/SMA membrane

The hydrophilicity of the membrane was characterized by a contact angle (CA) using a contact angle measuring instrument (OCA20, Germany). An approximate 5 μL deionized water droplet was dropped onto the dried flat membrane surface. Three measurements were taken for each sample and the average was calculated. In addition, the membrane was immersed in hydrochloric acid (0.1 mol L^{-1}) for 12 h and then washed until neutral. After dried, it was measured again.

2.6. Performance of PVDF/SMA membrane

The pure water flux (PWF) of the membrane was measured via a self-made device using a cross-flow mode. Each membrane was initially pressurized at 0.15 MPa for approximately 30 min. The pressure then decreased to 0.1 MPa, i.e., the operating pressure, and began to collect water. The PWF was calculated using the following equation: $J_w = V/(A\Delta t)$, where J_w (L m^{-2} h^{-1}) is the PWF, V (L) is the volume of permeated water, A (m^2) is the membrane area and Δt (h) is the permeation time. After the measurement of the PWF, the feed solution was replaced by the bovine serum albumin (BSA) solution (1 mg mL^{-1}, pH = 7.0). The rejection of the BSA was calculated by the following equation: $R=(1-C_p/C_f)\times 100\%$, where R is the rejection of BSA and C_p (mg L^{-1}) and C_f (mg L^{-1}) are the BSA concentrations of permeation and feed solutions, respectively. They were measured with an ultraviolet-spectrophotometer (UV-9200) at a wavelength of 280 nm. Each sample was measured for three times.

3. Results and discussion

3.1. Compatibility between PVDF and SMA

The membrane formation process and membrane structure were influenced markedly by the compatibility between blend polymers [21,22]. Fig. 1 presents the DMA spectra, and the corresponding data are listed in Table 1. The temperature of the maximum tan δ value corresponds to the glass transition temperature (T_g). More specifically, the peak, approximately 195 °C, corresponds to the glass transition of the SMA. Two peaks of approximately −50 °C and 55 °C [25] corresponds to the β relaxation and α relaxation of the PVDF, respectively, for the pristine PVDF membrane. The β and α relaxations can be ascribed to the glass transition of the unconstrained chains in the amorphous domain and the relaxation of the constrained amorphous chains associated with the PVDF crystal, respectively [26]. For the PVDF/SMA blend membranes, the two adjacent peaks located between the peaks of the pristine PVDF and SMA indicate the partial compatibility between PVDF and SMA. The partial compatibility can be ascribed to the dipole–dipole type interaction caused by the electronic polarization between the C—F_2 of the PVDF and the C=O or the St of the SMA [23].

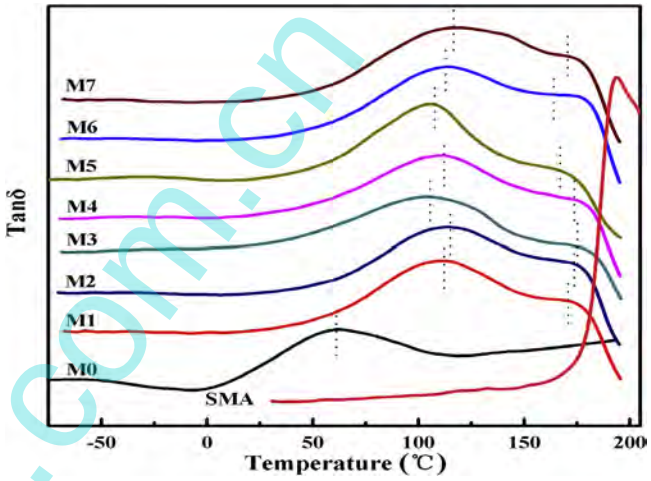

Fig. 1. DMA spectra of the PVDF/SMA blend membranes and SMA powder.

3.2. Phase diagram of PVDF/SMA/ATBC system

The cooling process of the PVDF/SMA/ATBC system is recorded using the polarizing optical microscope (POM). Fig. 2 presents the representative images (m0 and m3) at a reduced temperature. No liquid droplets produced by the coarsening of the polymer lean phase under the POM. However, the PVDF nucleation and crystallization growth during the polymer rich phase are observed under the POM. This suggests that the solid-liquid (S-L) phase separation and the PVDF crystallization occurs for all the system. Fig. 3 presents the final POM images of the system. The spherical structure with obvious Maltese extinction crosses are evident within the system without the blending of the SMA (m0). However, the Maltese extinction crosses become blurred with the addition of the

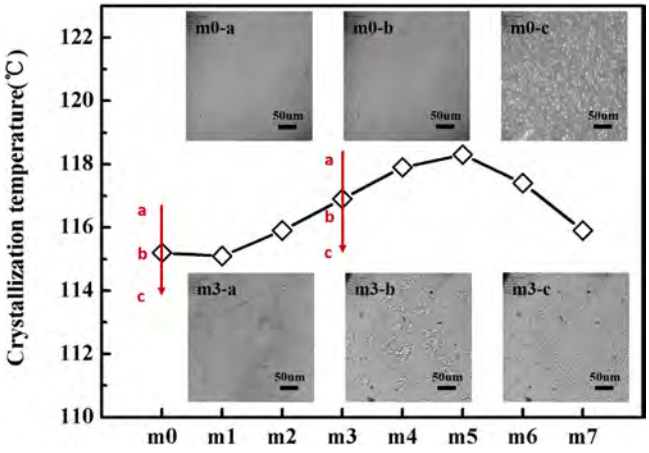

Fig. 2. Phase diagram of PVDF/SMA/ATBC system and representative micrographs measured by POM, homogeneous solution (a), the start of phase separation (b) and the final micrographs (c).

SMA (m1 to m7). Moreover, the spherulite size decreases and the number of spherulites increases (m1, m2 and m3) when a small amount of SMA is added. Furthermore, an increased amount of SMA is prone to agglomerate and form irregular spherulites (m4, m5, m6 and m7). This indicates that the PVDF crystallization is markedly influenced by the SMA content. It can be also seen from Fig. 2 that the crystallization temperature (T_c) of the system increases first and then decreases with the addition of the SMA. The influence of ATBC on T_c can be neglected because the weight ratio of PVDF is the same for different system if SMA is regarded as part of solvent. Therefore, the change in the T_c can mainly be ascribed to the synergistic effect among nucleation, compatibility and agglomeration of the SMA. When the SMA content is less than 3 wt.%, the stronger nucleation of the SMA and the poor compatibility between the PVDF and the SMA cause the PVDF to be prone to crystallization, thus increasing the T_c. Whereas an SMA content in the range of 3 wt.% to 5 wt.% results in better compatibility between the PVDF and the SMA and in the aggregation of the SMA hindering the crystallization of the PVDF, the effect of more SMA enhancing the PVDF nucleation is more obvious. Therefore, the T_c still increases. However, when the SMA content exceeds 5 wt.%, the compatibility between PVDF and SMA becomes better. The better compatibility and the formation of ensembles due to the aggregation of excess SMA surpasses the nucleation of the PVDF. Therefore, the T_c decreases.

3.3. Membrane morphology

Fig. 4 indicates the cross-section images of the membranes. It can be seen that the morphology changes from large spherulites to a network structure as the SMA content increases from 0 wt.% to 3 wt.%, after which it changes to irregular small spherulites as the SMA content further increases to 7 wt.%. In addition, the morphologies of the blended membranes are uniform and no obvious phase separation between the PVDF and the SMA. The spherulites of M0 further reveal that the PVDF/ATBC system undergoes an S-L phase separation, which is in accordance with the results of the POM in Fig. 3. The network structures for the samples of M1, M2 and M3 are also formed via the S-L phase separation because only PVDF crystallization can be observed under the POM. The network structure in this manuscript differs from the results reported in the literatures that the S-L phase separation forms the spherulite structure [27,28]. Compared with the M0, the size of the spherulites for the M4, M5, M6 and M7 samples is smaller, and the spherical shape becomes irregular.

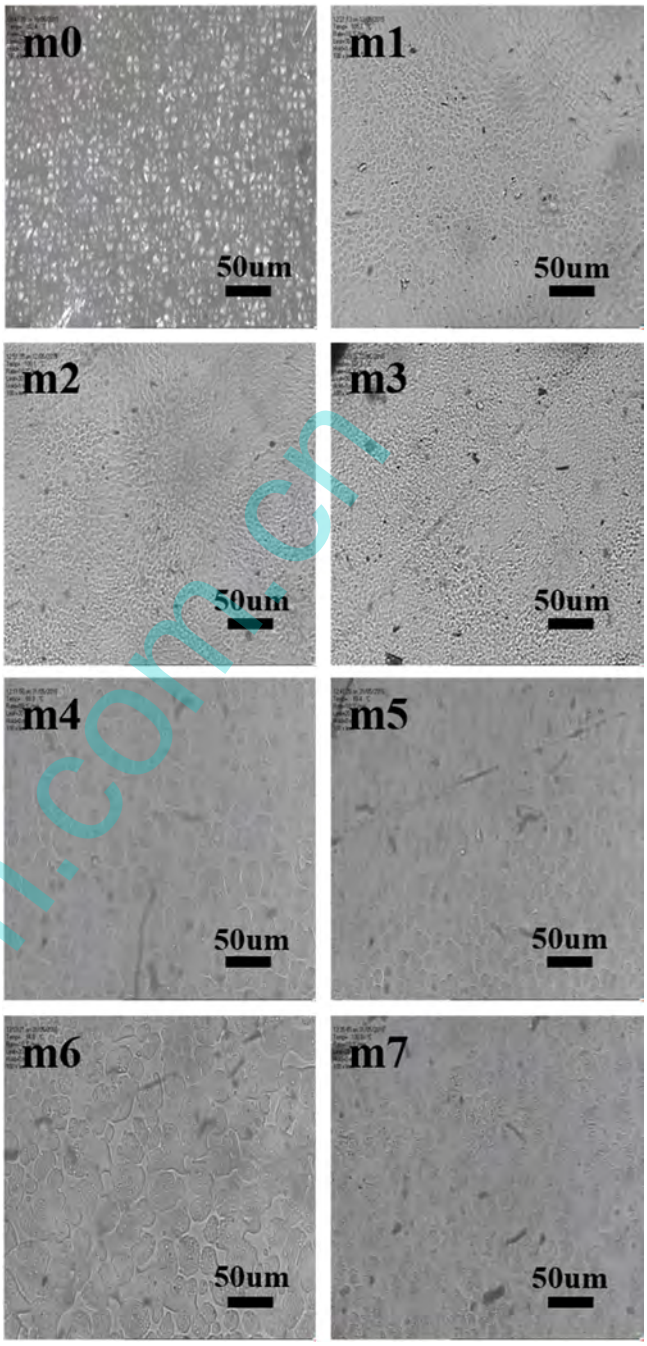

Fig. 3. Final micrographs of the PVDF/SMA/ATBC system at room temperature measured by POM on the cooling process.

DSC is used to analyse the change in morphology of the PVDF/SMA blend membranes, and the detailed data are listed in Table 1. It is evidenced that the values of ΔT_m and $T_m{}^p$ decrease first as the SMA content increases from 0 wt.% to 3 wt.% and then increases with the further addition of SMA. The $T_m{}^p$ and ΔT_m represent the thickness of the lamella and the distribution of the lamella thickness, respectively [29]. In other words, the decrease in ΔT_m and $T_m{}^p$ mean that the size of the PVDF microcrystal becomes smaller and more uniform. This is concordant with that of the SEM images in Fig. 4 as the network structure can be regarded as the interconnection of small and uniform lamella. The change in compatibility between the PVDF and SMA and the heterogeneous nucleation of the SMA further explains the change of morphology. As revealed in Fig. 1, as the SMA content increases from 0 wt.% to

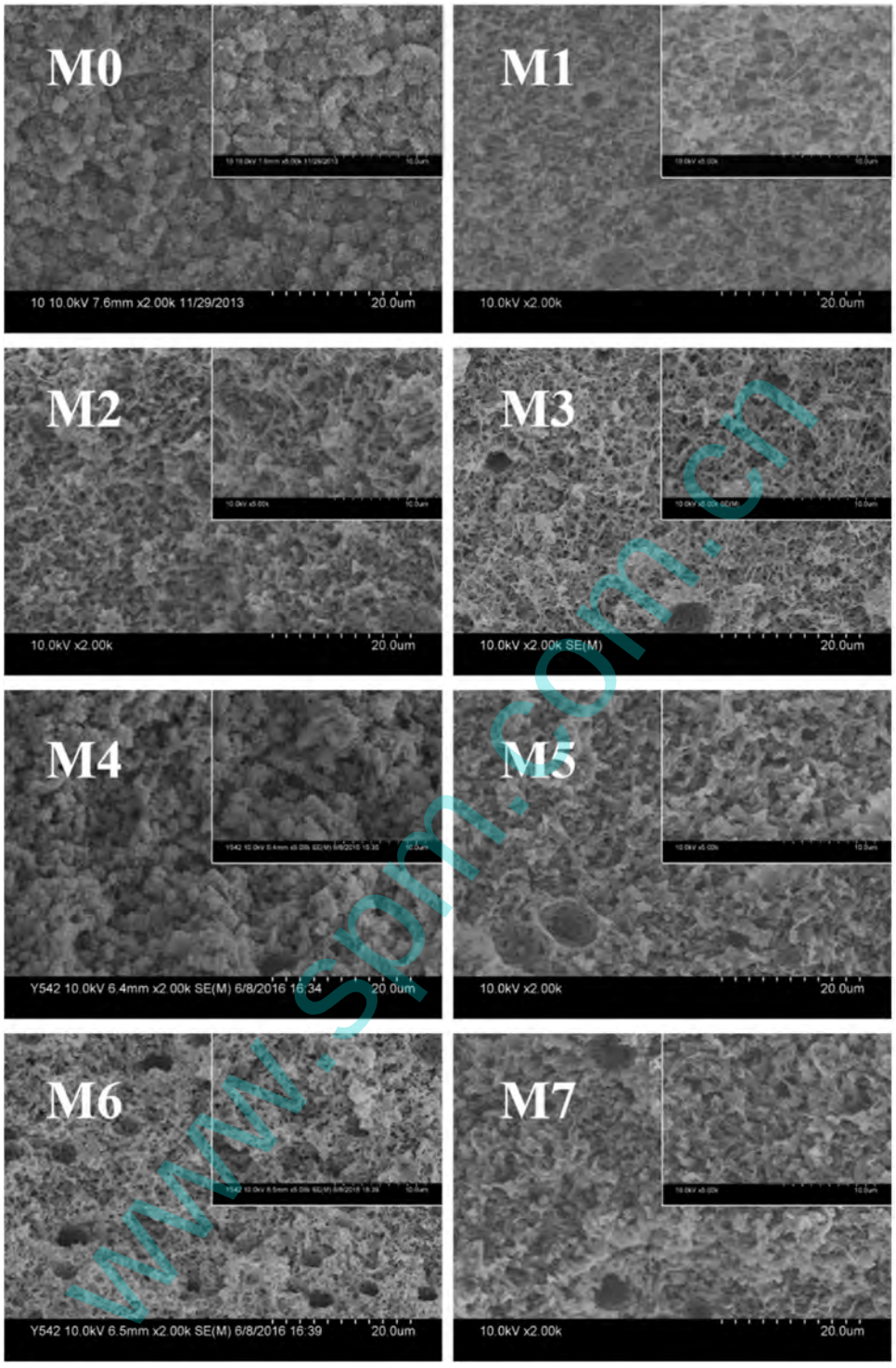

Fig. 4. The cross-section SEM of PVDF/SMA blend membrane.

3 wt.%, the poor compatibility facilitates PVDF nucleation and hinders growth, which results in a uniform and small microcrystal. However, as the SMA content increases from 3 wt.% to 7 wt.%, the aggregation of SMA and the better compatibility between PVDF and SMA hinders the nucleation of PVDF and results in a longer growth time, which then increases the size of the lamella and widens the distribution of lamella.

3.4. Surface deposition of SMA and membrane formation mechanism

Fig. 5 reveals the surface morphology and its surface pore size and its distribution [24] of the membrane. It is noted that the surface of the blend membrane was denser than that of the pristine membrane. In detail, the pore size became smaller and pore size distribution became narrower. In addition, compared to the pristine membrane (132 nm), the mean surface roughness (R_a) of the blend

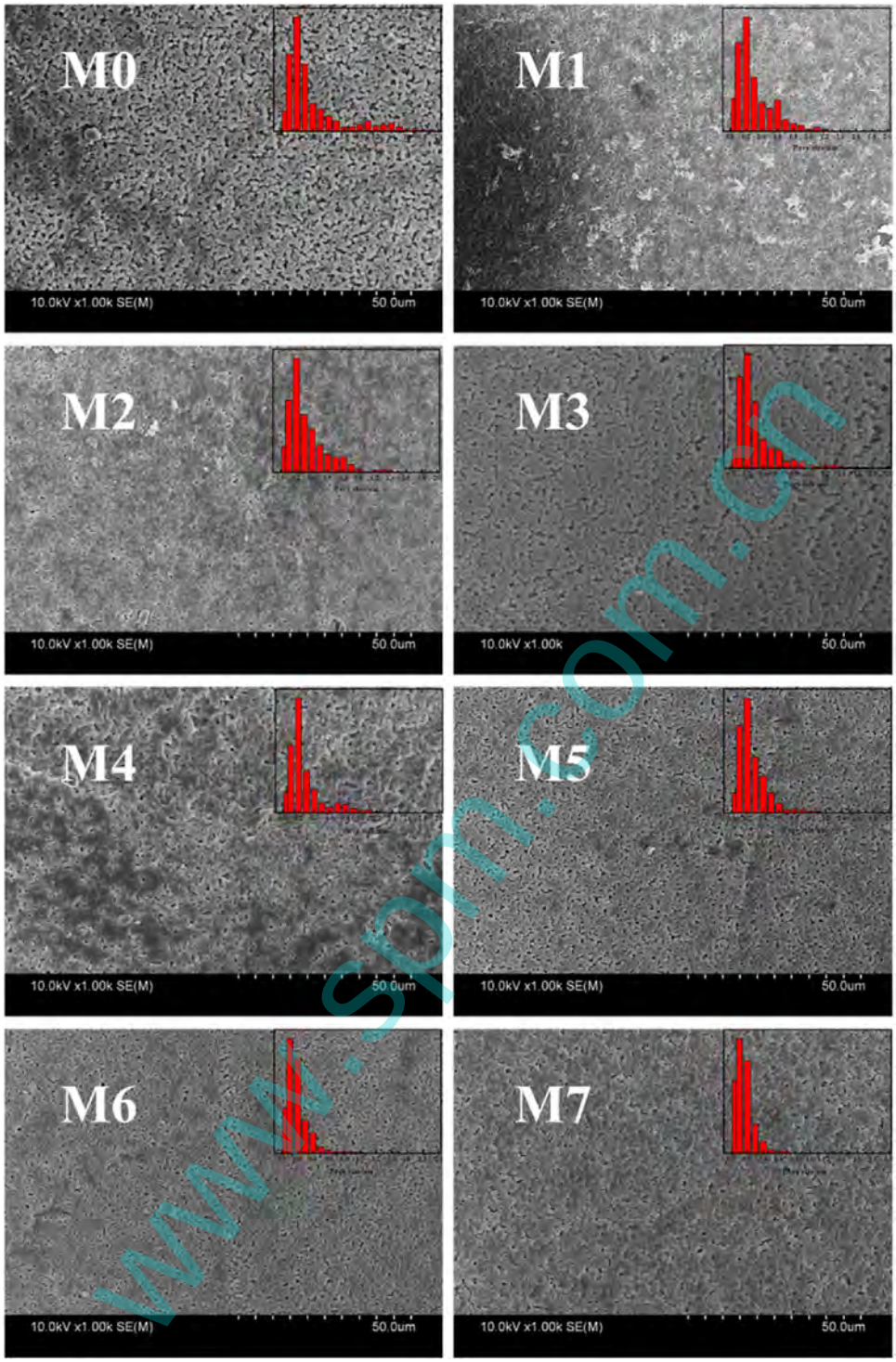

Fig. 5. Skin morphology of the membrane. Upper right is the surface pore size and its distribution.

membrane decreased (49.2 nm to 69.2 nm) (Table 2). The change in the surface morphology is ascribed to the surface deposition of the SMA.

The ATR-FTIR of the membranes is displayed in Fig. 6a. The characteristic peaks of anhydride (1779 cm^{-1} and 1858 cm^{-1}), carbonyl (1738 cm^{-1}) and styrene (1545 cm^{-1} and 1494 cm^{-1}) are found in the PVDF/SMA blend membrane [30]. This means that the SMA has been deposited on the established PVDF matrix. Moreover, the intensity of the characteristic peaks of anhydride (1779 cm^{-1} and 1858 cm^{-1}) by and large increased with the addition of the SMA. This is in accordance with the results presented in Fig. 5 that the surface becomes dense for the blend membrane. The XPS (Fig. 6b) of the three representative samples (M0, M3, and M7) is used to further characterize the composition of the deposited SMA on the skin layer. It is noted from the respective C_{1s} core-level spectra that there is an obvious increase in oxygen content and a corresponding decrease in fluorine content with an increase in SMA content for the PVDF/SMA membranes. For the pristine PVDF membrane (M0) of

Table 2
Membrane skin element compositions measured by XPS and its theoretical calculation and mean surface roughness measured by AFM (scan size is 8 um).

Membrane code	Experiment value [wt.%]		Theoretical value [wt.%]		Mean surface roughness [nm]	Porosity
	Oxygen (O)	Fluoride (F)	O	F		(%)
M0	2.83[a]	57.74	0	59.37	132	65
M1	3.97	55.21	0.9	54.99	67.2	70
M2	4.28	52.61	1.68	51.21	54.3	73
M3	6.07	49.7	2.36	47.92	49.2	75
M4	6.83	43.78	2.96	45.02	50.7	70
M5	9.56	29.6	3.48	42.45	57	68
M6	11.45	19.34	3.96	40.17	62.6	66
M7	12.82	16.43	4.38	38.11	69.2	63

a) The tiny amount of O element in PVDF powder may be due to the remaining surfactant where the details were not informed by the supplier.

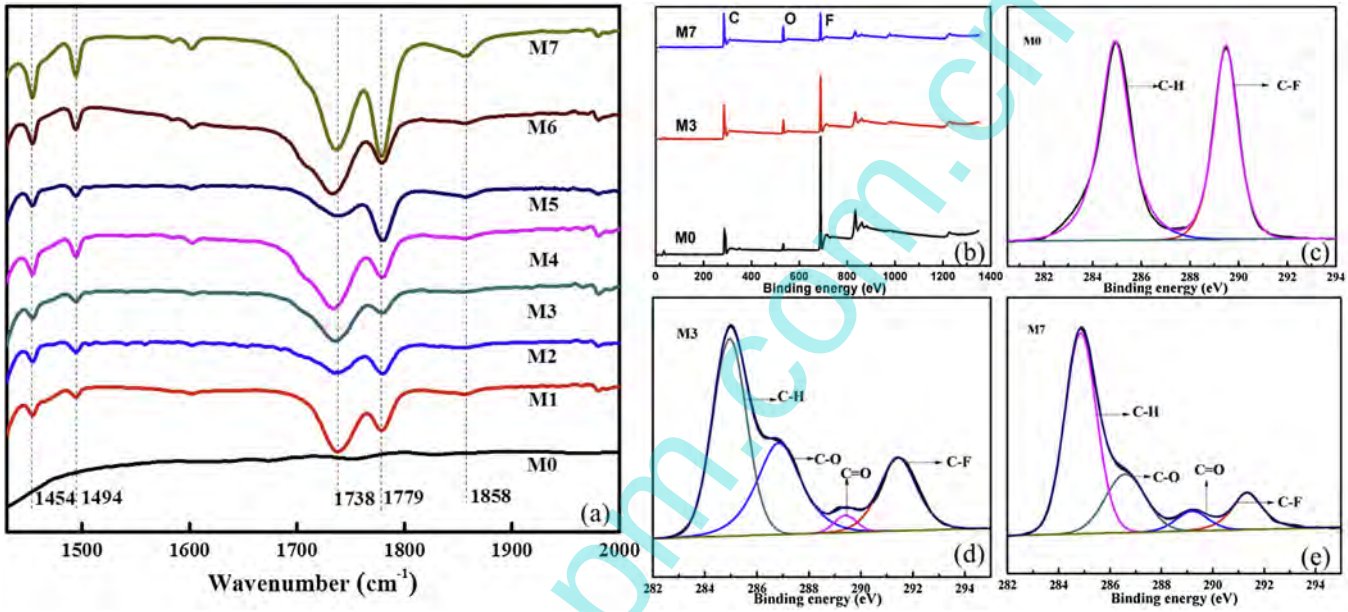

Fig. 6. ATR-FTIR spectra of PVDF/SMA blend membrane (a): M7′ represented the membrane (M7) after immersion in hydrochloric acid solution, XPS survey spectra (b) and XPS high-resolution C_{1s} spectra (c, d and e) of the representative PVDF/SMA blend membrane (M0, M3, M7).

the high-resolution XPS spectra of C_{1s} (Fig. 6c), the core-level spectrum can be curve-fitted with two peak components. The peaks of 286.4 and 290.9 eV represent the CH_2 and CF_2 groups, respectively. The ratio for the two peaks is approximately 1.03, which is in agreement with the structure of PVDF [23]. The three main peaks and one shoulder can be observed for the PVDF/SMA blend membranes, i.e., M3 and M7 in Fig. 6d and e. This means that, the peaks at 291.3 eV, 284.9 eV, 286.5 eV and 289.2 eV correspond to the C—F_2 bond, C—H bond, C—O and C=O function group, respectively [23]. Furthermore, it is noted that the experimental value of the oxygen content on the skin layer is approximately three times greater than that of the theoretical value (Table 2). And the maximum experimental value for surface segregation in Ref. [11] is approximately two times greater than the theoretical value. This indicates that compared with surface segregation, surface deposition can introduce more functional group onto the skin layer.

TEM was used to characterize the thickness of the surface deposition layer and the distribution of SMA within the PVDF matrix. Fig. 7 reveals the two representative cross-section TEM images of the PVDF/SMA membrane (M3 and M7). The black and grey domains represent SMA and PVDF, respectively. It can be seen that SMA not only deposits on the PVDF surface and forms a thin dense layer, but also distributes uniformly in the established PVDF matrix. Compared with the sample of M7, the distribution of SMA within the PVDF matrix for M3 is more uniform. The thickness of the SMA surface deposition layer is as thin as approximately 220 nm for M7 and a little thicker than that of M3 (approximately 200 nm). The TEM images indicate that the surface deposition offers a simple way to fabricate a uniform and thin functional layer on the surface of the membrane, which is difficult to realize using the traditional surface coating technique.

Based on the above discussions, the membrane formation mechanism, especially for the network structure supporting layer and the thin SMA deposition layer (M3), is illustrated in detail (Fig. 8). This TIPS-NIPS method can be interpreted as follows: In the cooling process, SMA not only acts as a nucleation reagent and facilitates PVDF nucleation, but also hinders the growth of PVDF. Thus, the PVDF crystallization only grows into lamella and the interconnection of the lamella forms the network structure in the polymer-rich phase. In the polymer-lean phase, the SMA dissolves in the ATBC. The diffraction between the ATBC and the ethanol leads to the NIPS process for the SMA/ATBC system during the extraction process and the SMA deposits on the skin layer and on the inner part of the established PVDF matrix when the extraction process is over. The partial compatibility between PVDF and SMA [23] prevents the SMA from peeling off.

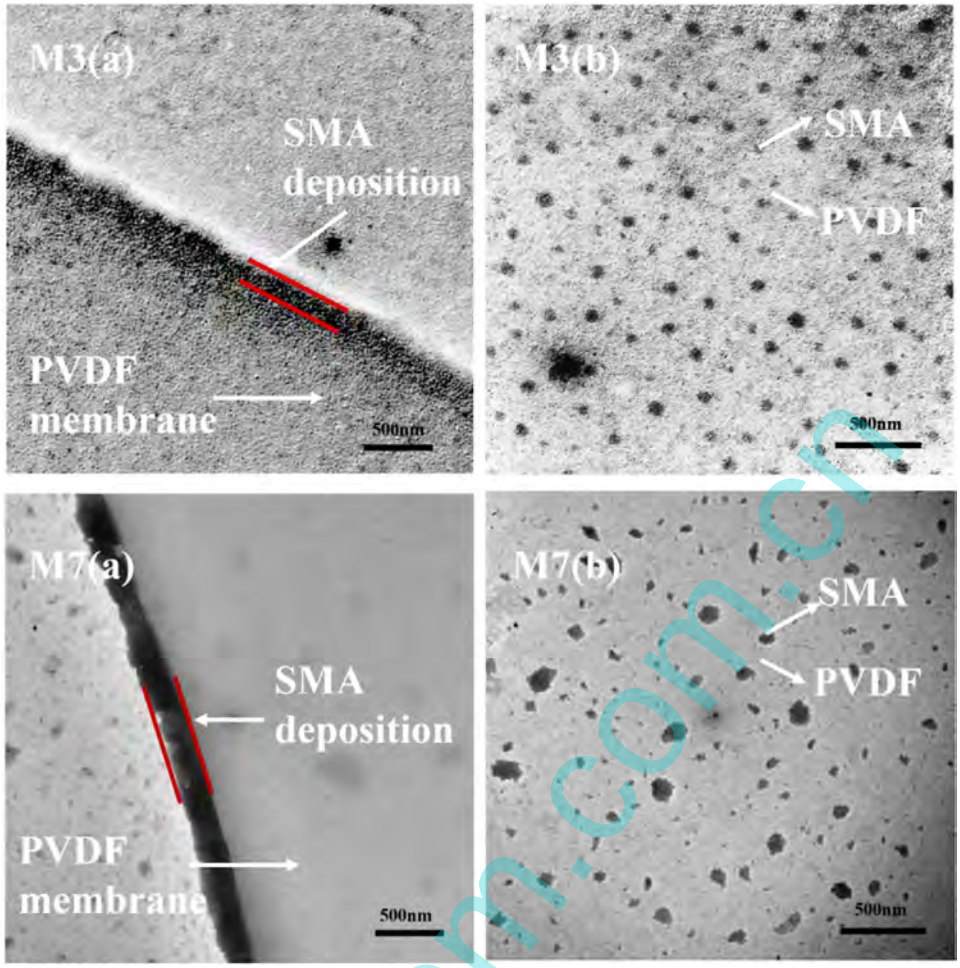

Fig. 7. Representative TEM cross-section images of the PVDF/SMA blend membrane (M3 and M7): close to the surface (a) and the middle part of the membrane (b).

3.5. Hydrophilicity of the membrane

The hydrophilicity of the membrane is evaluated based on the water contact angle (CA). As presented in Fig. 9, the value of the CA is about 112° for the pristine PVDF membrane (M0). The CA increases to 122° when the SMA content is 1 wt.% (M1) because the value of the CA is relevant to the surface roughness, hydrophilicity, porosity, pore size and pore size distribution of the membrane. If the surface layer of the membrane is highly porous, the value of the CA may become very low even though the membrane is not necessarily hydrophilic [31]. On one hand, a small amount of SMA does not markedly improve the hydrophilicity of the membrane, i.e., M1 remains hydrophobic. On the other hand, the deposition of SMA decreases the surface roughness (Table 2) and surface pore size (Fig. 5) of the membrane. Thus, the effect of surface pore size and surface roughness on the CA becomes more obvious, and the value of the CA increases. The value of the CA decreases from 122° to 81° as the SMA content increases from 1% to 7%. This can mainly be ascribed to the influence of the SMA content. The weak hydrophilic nature of anhydride results in a still higher CA for the PVDF/SMA blend membrane because the smallest value of the CA is as high as 81°. However, the CA decreases markedly after the PVDF/SMA blend membrane is immersed in the hydrochloric acid solution and the minimum value is as low as 55° when the SMA content is at 7 wt.%. This indicates better hydrophilicity of the membrane. The decrease of the CA can mainly be ascribed to the anhydride hydrolysis and the form of the hydrophilic maleic acid group in the hydrochloric acid [32].

3.6. Performance of the membrane

Fig. 10 presents the PWF and BSA rejection of the blend membrane after it is immersed in the hydrochloric acid solution. It is evidenced that the PWF increases with the addition of SMA and reaches its maximum, i.e., 130 L m^{-2} h^{-1}, when the SMA content is 2 wt.%. It then decreases as the amount of SMA increases. However, the BSA rejection continues to increase, reaching 94% when the SMA content is at 7 wt.%. The change of the BSA rejection can be attributed to the SMA deposition. As can be seen in Fig. 5, the pore size became smaller and pore size distribution became narrower with the increase of SMA. The change of the PWF can be ascribed to the surface hydrophilicity, porosity and surface pore size. The introduction of SMA improves the hydrophilicity and results in an increase of the PWF. Conversely, the deposition of SMA on the membrane surface blocks the skin layer pore, which in turn decreases the PWF and increases the rejection of BSA. When the SMA content is less than 2 wt.%, the hydrophilicity and the porosity of the membrane increase, thus the PWF increases. However, when the SMA content is more than 2 wt.%, the influence of surface pore size on the PWF becomes obvious and the porosity decreases, thus the PWF decreases. In addition, Pereira et al. prepared PVDF/SMA blend membrane by conventional NIPS used NMP as solvent [20]. However, the PWF is only 20 L m^{-2} h and the BSA rejection is 68%, which

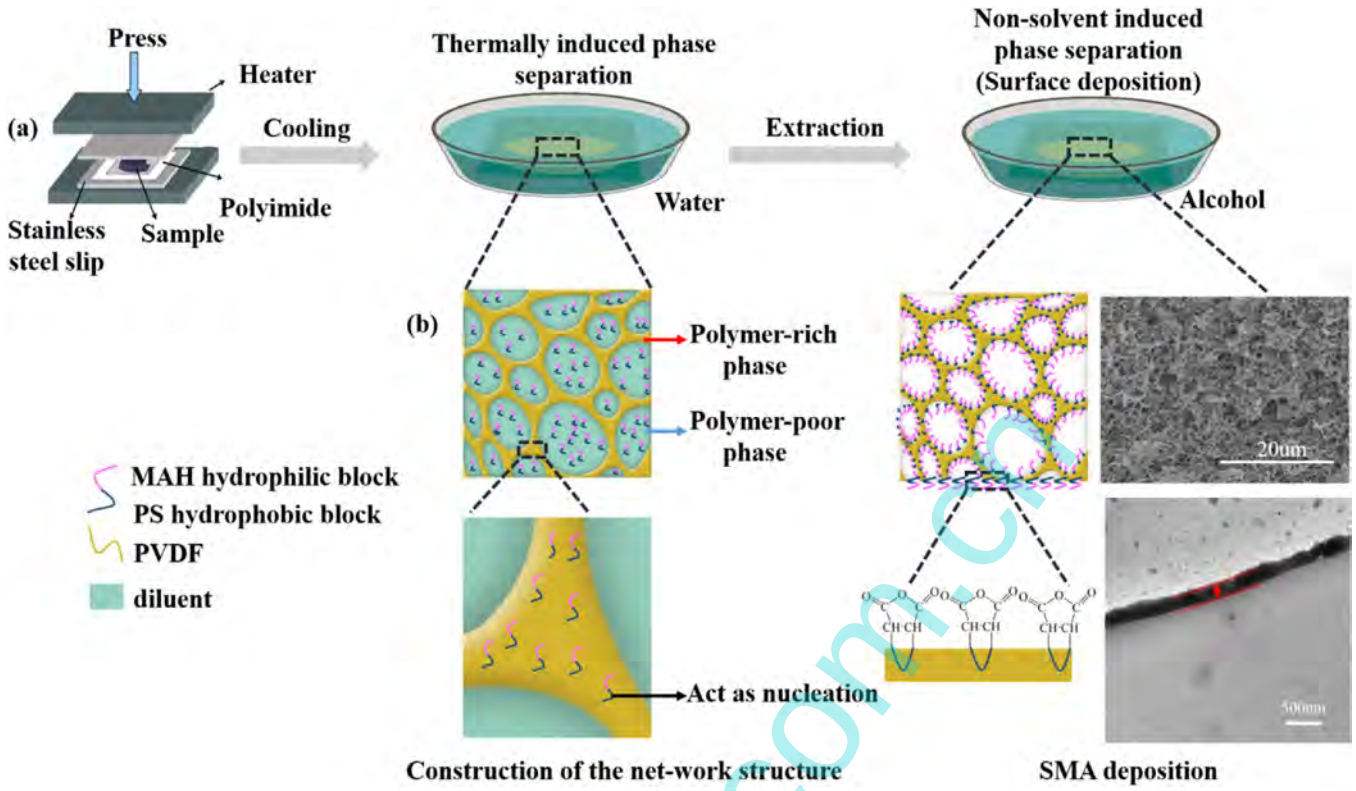

Fig. 8. The membrane fabrication process (a) and the scheme of membrane formation mechanism for skin deposition with network structure (b) for PVDF/SMA/ATBC system.

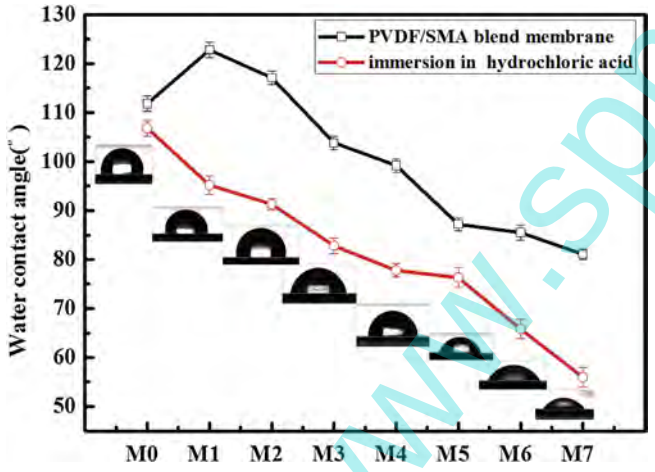

Fig. 9. Contact angle of PVDF/SMA blend membrane after immersed in hydrochloric acid solution.

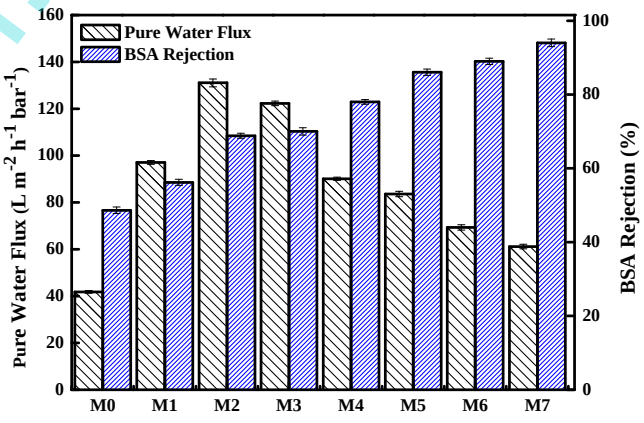

Fig. 10. PWF and BSA rejection of PVDF/SMA blend membrane.

are lower than the manuscript. This may be ascribed to the lower amount of SMA surface segregation, which in turn resulted in a no obvious modification effect. This further proved that the effect of hydrophilicity for surface deposition in this manuscript is better than that of surface segregation.

4. Conclusions

The PVDF-based blend membrane with a uniform SMA thin coating of approximately 200 nm was developed using the TIPS-NIPS process. The supporting layer with an interconnected network structure was formed using S-L phase separation of TIPS. This membrane formation mechanism, which can be ascribed to the effect of the SMA on PVDF crystallization and solubility in diluent, was proposed. The deposited SMA decreased the size of the membrane surface pore and increased hydrophilicity. The present investigation is beneficial for the simple fabrication of a thin functional skin layer and a network structure supporting layer.

Acknowledgements

This work was supported by the National Nature Foundation of China (No. 21576209), the Key Program of Science and Technology Foundation of Guizhou Province (No.[2016] 1405), the Program for Changjiang Scholars and Innovative Research Team in University (PCSIRT) of Ministry of Education of China (No. IRT13084) and Applied Basic Research and Advanced Technology Programs of Science and Technology Commission Foundation of Tianjin (No. 15PTSYJC00240). The author also thank for Waqar Iqbal and Xianhui Li.

References

[1] M.A. Shannon, P.W. Bohn, M. Elimelech, J.G. Georgiadis, B.J. Marinas, A.M. Mayes, Science and technology for water purification in the coming decades, Nature 452 (2008) 301–310.
[2] Z. Wang, W. Yu, C. Zhou, Preparation of polyethylene microporous membranes with high water permeability from thermally induced multiple phase transitions, Polymer 56 (2015) 535–544.
[3] K.V. Peinemann, V. Abetz, P.F.W. Simon, Asymmetric superstructure formed in a block copolymer via phase separation, Nat. Mater. 6 (2007) 992–996.
[4] J.F. Kim, J.H. Kim, Y.M. Lee, E. Drioli, Thermally induced phase separation and electrospinning methods for emerging membrane applications: A review, AIChE J. 62 (2016) 461–490.
[5] F. Liu, N.A. Hashim, Y. Liu, M.R.M. Abed, K. Li, Progress in the production and modification of PVDF membranes, J. Membr. Sci. 375 (2011) 1–27.
[6] Q. Zhou, Z. Wang, H. Shen, Z. Zhu, L. Liu, L. Yang, L. Cheng, Morphology and performance of PVDF TIPS microfiltration hollow fiber membranes prepared from PVDF/DBP/DOP systems for industrial application, J. Chem. Technol. Biotechnol. 91 (2016) 1697–1708.
[7] S. Liang, Y. Kang, A. Tiraferri, E.P. Giannelis, X. Huang, M. Elimelech, Highly hydrophilic polyvinylidene fluoride (PVDF) ultrafiltration membranes via postfabrication grafting of surface-Tailored silica nanoparticles, ACS Appl. Mater. Interfaces 5 (2013) 6694–6703.
[8] E.T. Kang, Y. Zhang, Surface modification of fluoropolymers via molecular design, Adv. Mater. 12 (2000) 1481–1494.
[9] T. Yuan, J. Meng, T. Hao, Z. Wang, Y. Zhang, A scalable method toward superhydrophilic and underwater superoleophobic PVDF membranes for effective Oil/Water emulsion separation, ACS Appl. Mater. Interfaces 7 (2015) 14896–14904.
[10] W.-Z. Qiu, H.-C. Yang, L.-S. Wan, Z.-K. Xu, Co-deposition of catechol/polyethyleneimine on porous membranes for efficient decolorization of dye water, J. Mater. Chem. A 3 (2015) 14438–14444.
[11] W. Chen, Y. Su, J. Peng, Y. Dong, X. Zhao, Z. Jiang, Engineering a robust, versatile amphiphilic membrane surface through forced surface segregation for ultralow flux-Decline, Adv. Funct. Mater. 21 (2011) 191–198.
[12] M.M. Pendergast, E.M.V. Hoek, A review of water treatment membrane nanotechnologies, Energy Environ. Sci. 4 (2011) 1946–1971.
[13] L. Wu, J. Sun, An improved process for polyvinylidene fluoride membrane preparation by using a water soluble diluent via thermally induced phase separation technique, Mater. Des. 86 (2015) 204–214.
[14] T. Xiao, P. Wang, X. Yang, X. Cai, J. Lu, Fabrication and characterization of novel asymmetric polyvinylidene fluoride (PVDF) membranes by the nonsolvent thermally induced phase separation (NTIPS) method for membrane distillation applications, J. Membr. Sci. 489 (2015) 160–174.
[15] T. Ishigami, Y. Nii, Y. Ohmukai, S. Rajabzadeh, H. Matsuyama, Solidification behavior of polymer solution during membrane preparation by thermally induced phase separation, Membranes 4 (2014) 113–122.
[16] S. Rajabzadeh, C. Liang, Y. Ohmukai, T. Maruyama, H. Matsuyama, Effect of additives on the morphology and properties of poly(vinylidene fluoride) blend hollow fiber membrane prepared by the thermally induced phase separation method, J. Membr. Sci. 423–424 (2012) 189–194.
[17] A. Qin, X. Wu, B. Ma, X. Zhao, C. He, Enhancing the antifouling property of poly(vinylidene fluoride)/SiO2 hybrid membrane through TIPS method, J. Mater. Sci. 49 (2014) 7797–7808.
[18] L.P. Zhu, X.X. Zhang, L. Xu, C.H. Du, B.K. Zhu, Y.Y. Xu, Improved protein-adsorption resistance of polyethersulfone membranes via surface segregation of ultrahigh molecular weight poly(styrene-alt-maleic anhydride), Colloids Surf. B 57 (2007) 189–197.
[19] T. Xiang, M. Tang, Y. Liu, H. Li, L. Li, W. Cao, S. Sun, C. Zhao, Preparation and characterization of modified polyethersulfone hollow fiber membranes by blending poly (styrene-alt-maleic anhydride), Desalination 295 (2012) 26–34.
[20] V.R. Pereira, A.M. Isloor, U.K. Bhat, A.F. Ismail, Preparation and antifouling properties of PVDF ultrafiltration membranes with polyaniline (PANI) nanofibers and hydrolysed PSMA (H-PSMA) as additives, Desalination 351 (2014) 220–227.
[21] M. Ting, C. Zhenyu, W. Ying, Q. Shuhao, W. Hong, Y. Feng, H. Na, L. Jianxin, Preparation of PVDF based blend microporous membranes for lithium ion batteries by thermally induced phase separation: I. Effect of PMMA on the membrane formation process and the properties, J. Membr. Sci. 444 (2013) 213–222.
[22] C. Qiao, C. Zhenyu, L. Jiangbo, Q. Shuhao, Y. Feng, L. Jianxin, Preparation and performance of polymer electrolyte based on poly(vinylidene fluoride)/polysulfone blend membrane via thermally induced phase separation process for lithium ion battery, J. Power Sources 266 (2014) 401–413.
[23] G.M. Qiu, L.P. Zhu, B.K. Zhu, Y.Y. Xu, G.L. Qiu, Grafting of styrene/maleic anhydride copolymer onto PVDF membrane by supercritical carbon dioxide: preparation, characterization and biocompatibility, J. Supercrit. Fluids 45 (2008) 374–383.
[24] R. Ziel, A. Haus, A. Tulke, Quantification of the pore size distribution (porosity profiles) in microfiltration membranes by SEM, TEM and computer image analysis, J. Membr. Sci. 323 (2008) 241–246.
[25] T. Ma, Z. Cui, Y. Wu, S. Qin, H. Wang, F. Yan, N. Han, J. Li, Preparation of PVDF based blend microporous membranes for lithium ion batteries by thermally induced phase separation: I. Effect of PMMA on the membrane formation process and the properties, J. Membr. Sci. 444 (2013) 213–222.
[26] J.F. Mano, V. Sencadas, A.M. Costa, S. Lanceros-Mendez, Dynamic mechanical analysis and creep behaviour of β-PVDF films, Mater. Sci. Eng. A A370 (2004) 336–340.
[27] G.L. Ji, L.P. Zhu, B.K. Zhu, C.F. Zhang, Y.Y. Xu, Structure formation and characterization of PVDF hollow fiber membrane prepared via TIPS with diluent mixture, J. Membr. Sci. 319 (2008) 264–270.
[28] B.J. Cha, J.M. Yang, Preparation of poly(vinylidene fluoride) hollow fiber membranes for microfiltration using modified TIPS process, J. Membr. Sci. 291 (2007) 191–198.
[29] X. Zhao, J. Cheng, S. Chen, J. Zhang, X. Wang, Controlled crystallization of poly(vinylidene fluoride) chains from mixed solvents composed of its good solvent and nonsolvent, J. Polym. Sci. Part B-Polym. Phys. 48 (2010) 575–581.
[30] G. Schoukens, J. Martins, P. Samyn, Insights in the molecular structure of low- and high-molecular weight poly(styrene-maleic anhydride) from vibrational and resonance spectroscopy, Polymer 54 (2013) 349–362.
[31] D. Rana, T. Matsuura, Surface modifications for antifouling membranes, Chem. Rev. 110 (2010) 2448–2471.
[32] C. Malardier-Jugroot, T.G.M. van de Ven, M.A. Whitehead, Study of the water conformation around hydrophilic and hydrophobic parts of styrene-maleic anhydride, J. Mol. Struct.: THEOCHEM 679 (2004) 171–177.